MOLECULAR AND CELLULAR BIOLOGY, May 2007, p. 3456–3469 Vol. 27, No. 9
0270-7306/07/$08.00+0 doi:10.1128/MCB.01719-06

Insulin Stimulates Membrane Fusion and GLUT4 Accumulation in Clathrin Coats on Adipocyte Plasma Membranes▽†

Shaohui Huang,[1] Larry M. Lifshitz,[2] Christine Jones,[1] Karl D. Bellve,[2] Clive Standley,[2] Sonya Fonseca,[1] Silvia Corvera,[1] Kevin E. Fogarty,[2] and Michael P. Czech[1]*

Program in Molecular Medicine, University of Massachusetts Medical School, 373 Plantation Street, Worcester, Massachusetts 01605,[1] *and Biomedical Imaging Group, Department of Physiology, University of Massachusetts Medical School, 373 Plantation Street, Worcester, Massachusetts 01605*[2]

Received 12 September 2006/Returned for modification 7 November 2006/Accepted 15 February 2007

Total internal reflection fluorescence (TIRF) microscopy reveals highly mobile structures containing enhanced green fluorescent protein-tagged glucose transporter 4 (GLUT4) within a zone about 100 nm beneath the plasma membrane of 3T3-L1 adipocytes. We developed a computer program (Fusion Assistant) that enables direct analysis of the docking/fusion kinetics of hundreds of exocytic fusion events. Insulin stimulation increases the fusion frequency of exocytic GLUT4 vesicles by ~4-fold, increasing GLUT4 content in the plasma membrane. Remarkably, insulin signaling modulates the kinetics of the fusion process, decreasing the vesicle tethering/docking duration prior to membrane fusion. In contrast, the kinetics of GLUT4 molecules spreading out in the plasma membrane from exocytic fusion sites is unchanged by insulin. As GLUT4 accumulates in the plasma membrane, it is also immobilized in punctate structures on the cell surface. A previous report suggested these structures are exocytic fusion sites (Lizunov et al., J. Cell Biol. 169:481–489, 2005). However, two-color TIRF microscopy using fluorescent proteins fused to clathrin light chain or GLUT4 reveals these structures are clathrin-coated patches. Taken together, these data show that insulin signaling accelerates the transition from docking of GLUT4-containing vesicles to their fusion with the plasma membrane and promotes GLUT4 accumulation in clathrin-based endocytic structures on the plasma membrane.

The concentration of glucose transporter 4 (GLUT4) in the plasma membrane (PM) determines the rate of glucose metabolism in adipose and muscle cells, which in turn contributes to whole-body glucose homeostasis. Cellular GLUT4 is dynamically distributed among the PM and various intracellular membrane compartments (7). Insulin stimulation significantly increases the exocytic rate of GLUT4 vesicles while modestly inhibiting GLUT4 endocytosis, resulting in >10-fold increases in PM GLUT4 in primary adipocytes (7, 24). Insulin signaling mobilizes a population of specialized insulin-responsive GLUT4 vesicles (IRVs) towards the PM, potentially through motor protein activities of KIF3 and KIF5B kinesins on microtubules (19, 39). Near the PM, a cortical F-actin network and unconventional myosin 1c promote GLUT4 vesicular trafficking and fusion (5, 18). Subsequent membrane fusion events are mediated by soluble *N*-ethylmaleimide-sensitive factor attachment protein receptor (SNARE) core proteins syntaxin 4, vesicle-associated membrane protein 2, and synaptosome-associated protein 23 (12, 43). The SNARE core is energetically extremely stable; thus, the timing of its formation and subsequent dissociation is likely regulated by SNARE-associated proteins, such as Munc-18c, tomosyn, synip, and pantophysin (43). Recently Lizunov et al. applied total internal reflection fluorescence (TIRF) microscopy to this problem in primary fat cells (30). Insulin reduces the average distance GLUT4 vesicles travel in the TIRF evanescence field. These results, indicating immobilization of GLUT4 by insulin, are interpreted by the authors to reflect tethering of exocytic GLUT4 vesicles to the PM prior to membrane fusion (30).

Retrieval of GLUT4 from the PM is mediated through the clathrin-mediated endocytic pathway (35, 25), as well as a cholesterol-dependent pathway (3). Interestingly, GLUT4 internalization in the basal state is reported to be mostly through the latter pathway, which is inhibited by insulin (3). These novel findings indicate that insulin signaling to inhibit cholesterol-dependent endocytosis contributes significantly to the accumulation of GLUT4 on the PM. Beyond that, molecular mechanisms governing GLUT4 transitions through the early endosomal compartments are largely unknown, with Rab5 and EH domain-containing protein 2 being recently implicated in these processes (15, 17). While part of this endocytic pool of GLUT4 is recycled back to the PM through the general endosomal recycling compartments, the majority of internalized GLUT4 molecules are proposed to replenish IRVs (16, 28). It is still debated whether the trans-Golgi network is involved in GLUT4 sorting from endosomes to IRVs (7, 26). Recent evidence suggests that the Golgi compartment-localized, gamma-ear-containing, ADP ribosylation factor-binding protein GGA is responsible for targeting newly synthesized GLUT4 to IRVs (44). Intriguingly, GGA also appears to be involved in converting endocytic GLUT4 vesicles to IRVs (29).

A critical unanswered question about GLUT4 trafficking is the site or sites along the membrane recycling pathway that are regulated by insulin. In order to further analyze GLUT4 dynamics near the PM, we used a custom-built two-color TIRF

* Corresponding author. Mailing address: Program in Molecular Medicine, University of Massachusetts Medical School, 373 Plantation Street, Worcester, Massachusetts 01605. Phone: (508) 856-2254. Fax: (508) 856-1617. E-mail: michael.czech@umassmed.edu.

† Supplemental material for this article may be found at http://mcb.asm.org/.

▽ Published ahead of print on 5 March 2007.

microscope to investigate GLUT4 trafficking in cultured 3T3-L1 adipocytes. Insulin promotes a ~3.0-fold increase of enhanced-green-fluorescent-protein (EGFP)-tagged GLUT4 (GLUT4-EGFP) fluorescence in the TIRF evanescence field, which is accompanied by apparent immobilization of punctate GLUT4 structures. Two-color TIRF microscopy of adipocytes coexpressing EGFP-tagged GLUT4 and dsRed-tagged clathrin light chain indicates that the immobilization effect is largely due to insulin-induced GLUT4 accumulation in immobile clathrin-coated pits rather than in exocytic GLUT4 vesicles. When TIRF imaging was carried out at 10 frames per second (fps), abundant single-vesicle fusion events were resolved in insulin-stimulated adipocytes, with many fewer fusion events detected in unstimulated cells. Importantly, all fusion processes are completed within ~1 s and are preceded by vesicle docking periods typically lasting a few seconds. We have developed a computer program (Fusion Assistant) that facilitates analysis of hundreds of single-vesicle docking/fusion kinetics. We found insulin increases GLUT4 vesicle fusion frequency by ~4-fold while substantially decreasing the vesicle-docking duration. These results provide direct evidence with live cells supporting insulin regulation of the GLUT4 vesicle docking/fusion mechanism at the PM.

MATERIALS AND METHODS

Plasmid constructs, cell culture, and plasmid transfection. The Myc- and EGFP-tagged GLUT4 construct has been described previously (23). This construct was digested with EcoR1 and Xba1 to replace the EGFP tag with monomeric red fluorescence protein 1 (mRFP1). The previously characterized dsRed-tagged clathrin light chain construct is a generous gift from Wolfhard Almers (32), and the EGFP-tagged clathrin light chain is from our colleagues (2). 3T3-L1 fibroblasts were grown to confluence and differentiated as described previously (18). About 4×10^6 adipocytes differentiated for 7 days were electroporated using Amaxa (Gaithersburg, MD) Nucleofector in a 0.1-ml transfection solution containing one or two of the above plasmid constructs (2 to 4 μg per construct per transfection). The cells were divided and plated into four to eight MatTek (Ashland, MA) culture dishes with a 10-mm-diameter coverslip (no. 1.5) bottom. After overnight cell culture and on the day of TIRF microcopy, transfected adipocytes in each dish were serum starved for >2 h before being switched into 2 ml KRH buffer (125 mM NaCl, 5 mM KCl, 1.3 mM $CaCl_2$, 1.2 mM $MgSO_4$, 20 mM D-glucose, 25 mM HEPES [pH 7.4], 0.2% [wt/vol] bovine serum albumin). TIRF imaging was typically carried out in this medium for 5 min, followed by 15 min of stimulation with 100 nM human insulin (Eli Lilly, Indianapolis, IN).

TIRF microscopy. The custom-built TIRF microscope has been described previously (2). The incident angle at the glass-water interface was measured using a previously described method (38), from which a typical evanescent field depth of ~100 nm was estimated. Two Coherent (Santa Clara, CA) Innova 70C lasers, argon (488-nm line) and argon-krypton (568 nm line), excite the EGFP and mRFP1/dsRed-tagged fusion proteins, respectively. The resulting fluorescence passes through a 488-568PC dichroic mirror (Chroma, Rockingham, VT), and EGFP and mRFP1/dsRed signals were selected using HQ525/50 band-pass (Chroma) and 3RD590LP long-pass (Omega Optical, Brattleboro, VT) filters, respectively. Due to chromatic aberrations, the red image was focused ~0.4 μm below the green image, which was corrected by a piezoelectric driver (E-662 LVPZT-Amplifier; PI GmbH & Co., Waldbronn, Germany) coupled to the objective. Thus, for a two-color TIRF experiment, one image was taken with an 80-ms exposure, followed by a 200-ms interval during which the laser light and its matching emission filter were selected and the correspondent focal plane piezoelectrically adjusted before another 80-ms exposure for the second image. The TIRF microscope is equipped with a Nikon 60× 1.45-numerical-aperture objective, and the entire microscopic setup is enclosed in a heated chamber with the interior temperature maintained at 35°C. Resulting TIRF images have a 100-nm pixel size.

Image processing. The local Biomedical Imaging Group (http://invitro.umassmed.edu) developed the necessary algorithms and computer programs for this study. For each TIRF image, a 16-by-16-pixel region in its background was selected, within which the average intensity (<BI>) and its associated standard deviation (std) were calculated. A threshold intensity (i.e., TI = <BI> + 3 × std) was subtracted from the image, which eliminates ~99.7% background signals (Fig. 2A and B). The halo of scattered fluorescence surrounding the actual cell boundary was due to fluorescence scattering within the adipocyte and thus was included as the whole-cell fluorescence intensity (Fig. 2C). The procedures of isolating punctate GLUT4 and clathrin structures and creating the correspondent binary images are demonstrated and described in detail in Fig. S1 in the supplemental material. Briefly, the edges of punctate GLUT4 structures (see Fig. S1A in the supplemental material) were enhanced using the differentiation-of-Gaussian algorithm (see Fig. S1B in the supplemental material). Subsequently, a mask was created in which pixels within the edges have a uniform intensity of 1 and those outside the edges have a uniform intensity of 0 (see Fig. S1C in the supplemental material). Applying (i.e., multiple) the mask to the original image separated out the punctate GLUT structures (e.g., see Fig. S1D in the supplemental material). An individual GLUT4 structure is defined as a local intensity maximum where the pixel intensity is higher than or equal to those of all its eight immediate neighbors. Applying this rule to isolated regions containing punctate GLUT4 structures (e.g., see Fig. S1D in the supplemental material), a computer program automatically identifies all possible individual GLUT4 structures (e.g., see red dots in Fig. S1E in the supplemental material).

Fusion Assistant. Using the procedures described above, all possible GLUT4 vesicles were identified for every TIRF image acquired using the burst protocol at 10 fps (illustrated in Fig. 8). Starting from the first image of the TIRF image sequence (e.g., 3,200 images acquired in 4 min of burst imaging after insulin addition), a trajectory of single-vesicle movements in the TIRF evanescence field was constructed by mapping a GLUT4 "vesicle" to its nearest neighbor in the next TIRF image acquired 0.1 s later. The trajectory was stopped when no "vesicle" was found within a circle of 1-pixel radius centered at the previous "vesicle" position. This procedure was repeated for every possible GLUT4 "vesicle" using a greedy-matching algorithm (9). Subsequently, each single-vesicle trajectory was screened for a possible fusion event based primarily on three rules derived from quantitative characterization (e.g., see Fig. 6; also see Fig. S5 in the supplemental material) of dozens of manually identified fusion events occurring in both quiescent and insulin-stimulated adipocytes. Development of Fusion Assistant is described in further detail in Results and Discussion (see Fig. 7; also see Movies S9 and S10 in the supplemental material).

Correcting random pixel colocalization. Two images (Im1 and Im2) have the same dimensions and M pixels in each image. N1 and N2 are randomly distributed pixels with positive pixel intensities in Im1 and Im2, respectively. Thus, the numbers of randomly colocalized, positive pixels are (N1/M)(N2/M)M = (N1 × N2)/M. The percentage of randomly colocalized positive pixels in Im1 is [(N1 × N2)/M/N1] × 100% = [N2/M] × 100%.

RESULTS

TIRF microscopy reveals abundant punctate GLUT4 structures beneath the PM of 3T3-L1 adipocytes. Cultured adipocytes transiently expressing GLUT4-EGFP were imaged with wide-field (Fig. 1A) and TIRF (Fig. 1B) microscopy while focusing on the coverslip-attached PM. With a high numerical aperture objective, wild-field imaging typically resolves structural details within a ~1-μm vertical slice of the adipocyte (Fig. 1A) (36). However, fluorescence signals originating outside of this ~1-μm section are also captured in the image, resulting in a mostly uniform background that blurs the resolved structural details (Fig. 1A). In contrast, the TIRF evanescence field decays exponentially from the coverslip-water interface. Thus, only fluorophores within a ~100-nm zone extending from the PM (Fig. 1) are sufficiently excited so that their fluorescence signals are resolved in the TIRF image (Fig. 1B). This vastly improved signal-to-background ratio reveals many punctate, vesicle-like structures containing GLUT4-EGFP fluorescence just beneath the PM (Fig. 1B), which have also been detected in previous TIRF studies of cultured and primary adipocytes (30, 41). These punctate GLUT4 structures could be related to multiple trafficking events, such as exocytic vesicle tethering/docking, vesicle fusion, clathrin-mediated endocytosis, and ves-

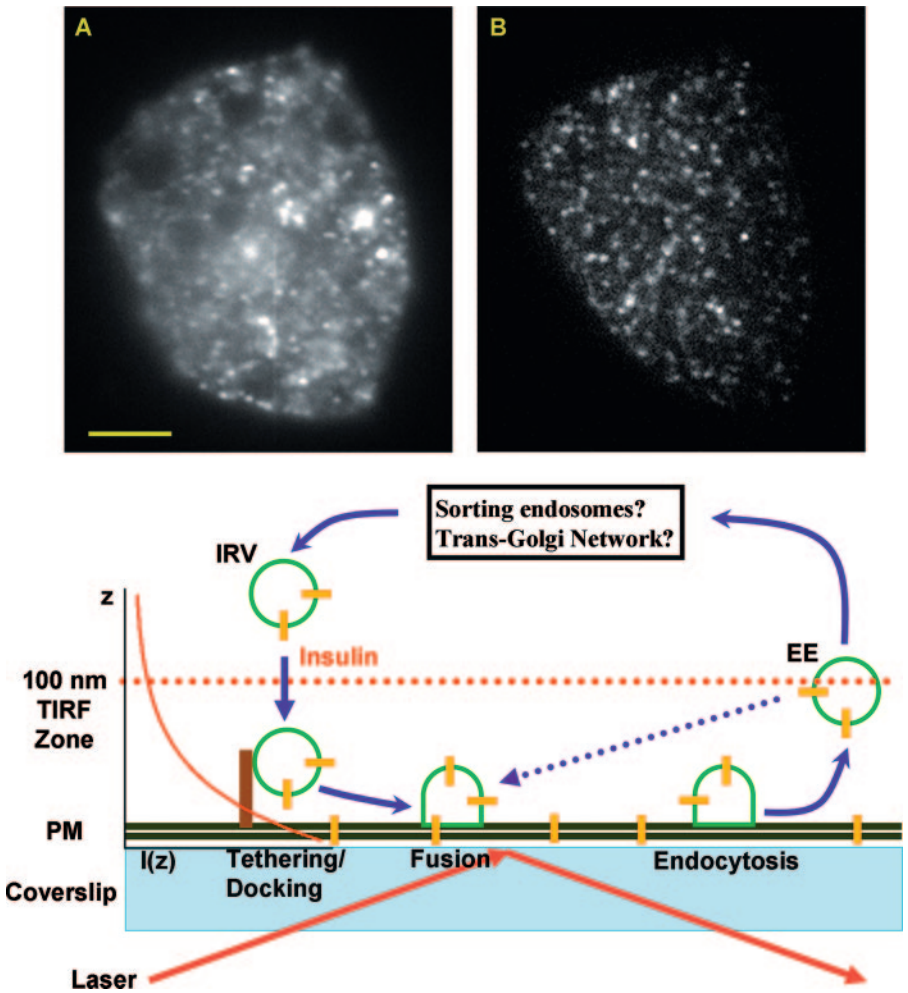

FIG. 1. TIRF microscopy reveals abundant GLUT4 vesicles underneath the PM of 3T3-L1 adipocytes. Both the wide-field (A) and TIRF (B) images are taken from the same adipocyte while focusing on the coverslip-attached PM. Scale bar in panel A, 5 μm. The TIRF evanescence field decays exponentially according to the equation $I(z) = I(0) \times \exp(-z/D)$, where $I(0)$ and $I(z)$ are excitation intensities at the coverslip-water interface and at z distance away from that interface, respectively (see diagram at right side of the cartoon illustration). The characteristic penetration depth (D) of the TIRF evanescence field is typically measured to be ~100 nm (see Materials and Methods). Thus, within this field, exocytic vesicle docking and fusion, as well as GLUT4 endocytosis, can be observed (see illustration). Insulin mobilizes intracellular insulin-responsive, GLUT4-containing vesicles (IRVs) towards the PM. The dotted blue line suggests a potential "short-circuit" pathway through which GLUT4-containing early endosomes (EEs) recycle back to the PM without going through intracellular sorting compartments (see black box).

icles constantly entering and leaving the TIRF evanescence field (see model in Fig. 1).

Insulin promotes GLUT4 exocytosis to the PM. Representative TIRF images acquired before and after insulin addition are shown in Fig. 2A and B, respectively. There are hundreds of punctate GLUT4 structures in the TIRF evanescence field of a quiescent adipocyte (Fig. 2A), and rapid movements associated with most of these structures suggest they are not tethered/docked to the PM (see Movie S1 in the supplemental material). There is little diffuse GLUT4-EGFP fluorescence in the background (Fig. 2A), suggesting a low GLUT4 presence in the PM. Thus, in quiescent adipocytes, either GLUT4 vesicle fusion with the PM is effectively blocked or subsequent GLUT4 endocytosis is very efficient, or both. Insulin promotes a dramatic increase in the total and diffuse GLUT4-EGFP fluorescence in the TIRF evanescence field (compare Fig. 2A and B) (see Movie S1 in the supplemental material). This is accompanied by the appearance of an extended cell surface area (the initial cell boundary is outlined in Fig. 2A and B) and dramatic membrane ruffling events (see Movies S1 and S3 in the supplemental material). Quantification of fluorescence changes indicates a ~3.0-fold increase of total GLUT4-EGFP signal in the TIRF evanescence field for the whole cell and a ~2.5-fold increase within the initial cell boundary (Fig. 2C).

Average results from eight adipocytes indicate a ~3.0-fold fluorescence increase for the entire cell boundaries and a ~2.6-fold increase within the initial cellular boundaries (Fig. 2D). These increases represent higher insulin responses than the 1.3- to 2.2-fold increases obtained from previous TIRF studies using 3T3-L1 adipocytes expressing GLUT4-EGFP constructs (13, 41). Nevertheless, such fluorescence enhancements in the TIRF evanescence field are significantly smaller than the correspondent 5- to 10-fold increases in the cell surface-exposed GLUT4 content estimated using three different

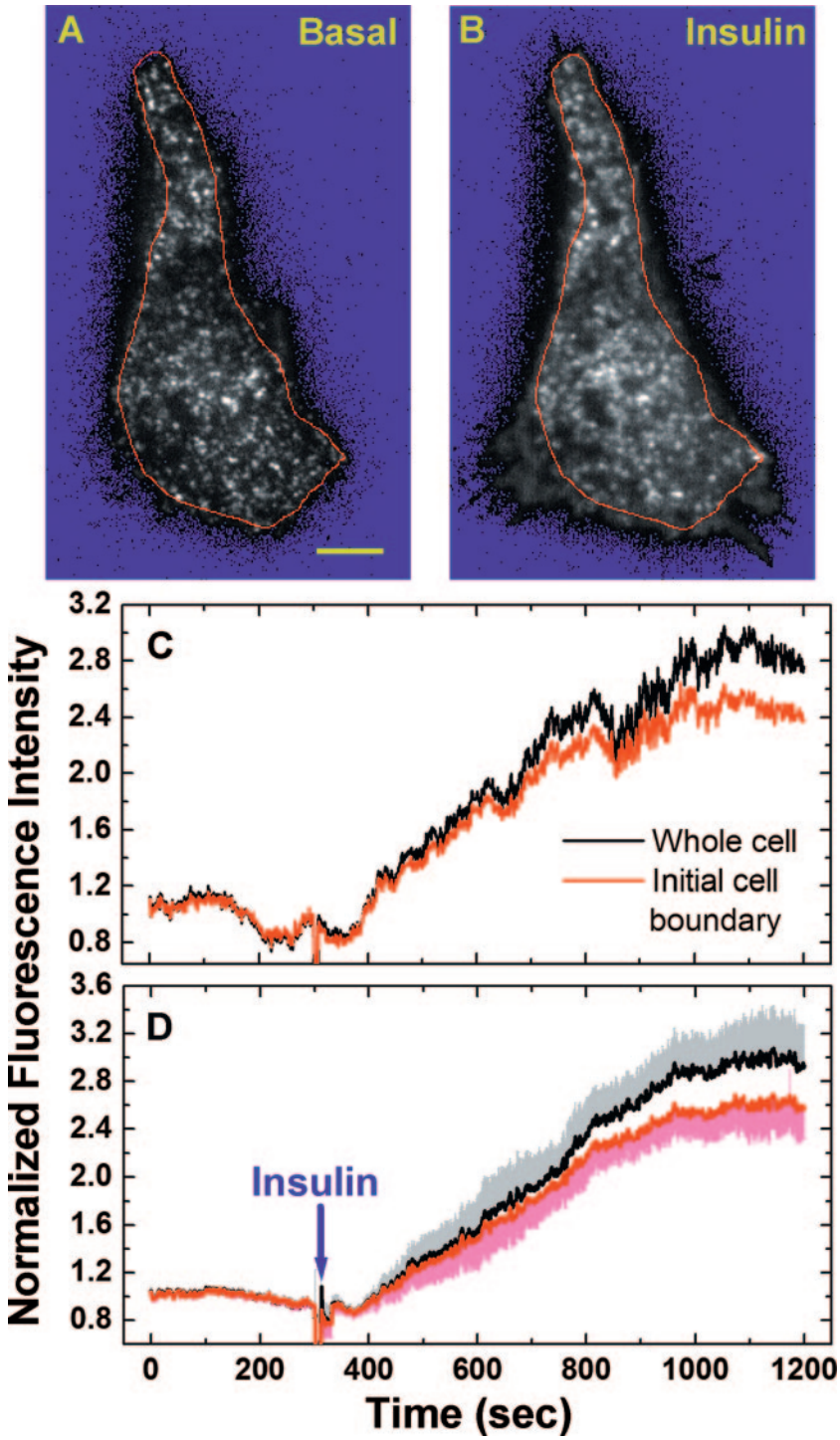

FIG. 2. Insulin stimulates GLUT4 exocytosis to the PM. Adipocytes transiently expressing GLUT4-EGFP were serum starved >2 h (i.e., basal conditions) before TIRF microscopy. Single-cell imaging was carried out at 1 fps for 5 min under the basal conditions, followed by 15 min of stimulation with 100 nM insulin (see Movie S1 in the supplemental material). Thus, a total of 1,200 images (i.e., img1 to img1200) were acquired, and img3 (A) and img902 (B) are representative cell conditions before and after insulin stimulation, respectively. Scale bar in panel A, 5 μm. After subtracting background signals (see the resulting blue background in panels A and B), remaining fluorescence intensities of the whole cell or within the initial cell boundary (i.e., red lines in A and B) were normalized to their respective average intensities before insulin addition and were plotted in panel C. The average insulin-induced fluorescence intensity changes for eight adipocytes are plotted in panel D, together with the standard errors of the mean.

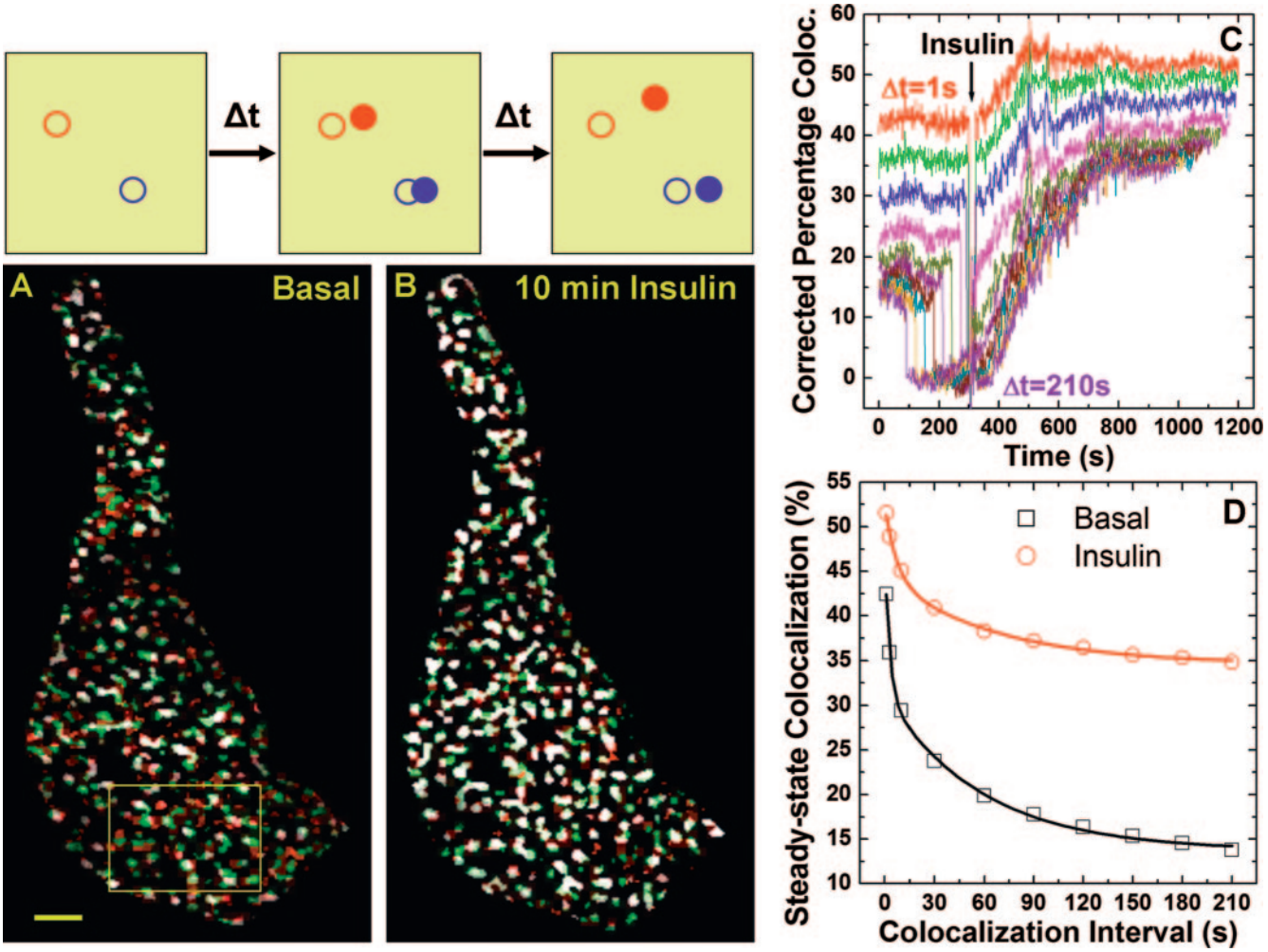

FIG. 3. Insulin promotes apparent immobilization of punctate GLUT4 structures. The principle of estimating vesicle mobility based on temporal colocalization (coloc.) between pairs of images separated by Δt is illustrated. For example, a fast-moving vesicle (red circles) has already moved away from its original position (open red circle) over Δt, while a slow-moving vesicle (blue circles) still partially overlaps with its original position (open blue circle). Over $2\times$ Δt, both vesicles have no colocalization with their original positions. Thus, the degree of temporal colocalization is inversely related to vesicle mobility. To eliminate colocalization of background signals, GLUT4-containing structures were first isolated from each TIRF image using algorithms demonstrated in Fig. S1 in the supplemental material. The initial cell boundary outlined in Fig. 2 is used to retain the same area for colocalization analysis. Image A shows colocalized regions (white) between two images acquired under basal conditions and separated by 1 s ($\Delta t = 1$ s; green, early image [EI]; red, later image [LI]). Ten minutes after insulin addition, such colocalized regions (white) increase dramatically (B). Scale bar in panel A, 2 μm. Colocalization details within a magnified segment of the cell (box in A) for the entire image sequence (i.e., img1 versus img2, img2 versus img3 . . . img1199 versus img1200) are included in Movie S2 in the supplemental material. PC is defined as the percentage of pixels in EI colocalizing with pixels in LI. The corrected PC values (corrected for random colocalization; see Materials and Methods) for Δt values of 1 s, 3 s, 10 s, 30 s, 60 s, 90 s, 120 s, 150 s, 180 s, and 210 s are computed for the whole image sequence and are plotted in panel C. Increasing Δt values result in decreasing PC values (C). Thus, the average PC values before (averaged between 0 and 30 s in panel C) and after (averaged between 900 and 930 s in panel C) insulin addition are plotted against their respective Δt intervals in panel D. Lines in panel D represent nonlinear least-square fits of the data using a two-exponential decay model (see Fig. S2 in the supplemental material for detail).

quantitative GLUT4 translocation assays (4, 46, 14). Thus, it should be emphasized that TIRF microscopy measures the total fluorescence intensity of GLUT4-EGFP molecules distributed among the PM and various membrane structures attached to or immediately beneath the cell surface (Fig. 1). In contract, the aforementioned translocation assays detect only GLUT4 molecules incorporated into the PM with their exofacial loops exposed to extracellular antibody labeling.

Insulin promotes immobilization of punctate GLUT4 structures in the TIRF evanescence field. One of the most dramatic observations from our TIRF study is the apparent immobilization of rapidly moving GLUT4 into static punctate GLUT4 structures (see Movie S1 in the supplemental material). In a similar TIRF study using primary fat cells, Lizunov et al. also found that "insulin immobilizes GLUT4 vesicles into clusters on the PM" (30). We then developed a novel technique effective in quantifying these immobilized structures. The principle of estimating object mobility based on temporal colocalization of two images acquired with time interval Δt is illustrated and explained in Fig. 3. In such analysis, mobility of an object is

inversely related to the degree of colocalization between its temporal positions, and in TIRF microscopy, both vertical and lateral object movements will reduce such colocalization. Figures 3A and B show that colocalized punctate structures between pairs of images separated by 1 s (i.e., early image and later image) increase dramatically 10 min after insulin addition, indicating substantially reduced vesicle mobility. We further define percentage colocalization (PC) as the percentage of structural pixels in the early image colocalizing with those in the later image. This PC value is further corrected for the expected random colocalization (i.e., any two unrelated images have random colocalization; see Materials and Methods). Thus, the corrected PC values for the whole image sequence (i.e., 1,200 images per experiment [see Movie S1 in the supplemental material]) are computed for various Δt intervals, which are plotted in Fig. 3C. The steady-state PC levels before insulin addition decrease with increasing Δt (Fig. 2C), which is expected, because with dynamic GLUT4 structures, two images separated further in time will have less colocalization. Insulin changes the dynamics of punctate GLUT4 structures, and new steady-state PC levels are established within 500 s of insulin addition (Fig. 3C). For a Δt value of >10 s, some corrected PC values temporarily drop to zero before insulin addition. This is caused by temporal colocalization of images acquired before and after insulin addition, respectively. Addition of insulin slightly shifts subsequent TIRF images in lateral directions (see Fig. 4C and F), and punctate GLUT4 structures also rearrange themselves in response to insulin (see transitions to new steady-state PC levels in Fig. 3C). The fact that these corrected PC values do not significantly deviate below zero validates our method for subtracting random colocalization, since there cannot be negative colocalization.

The decay of steady-state PC levels with increasing Δt values contains dynamic information about the punctate GLUT4 structures. Thus, we plotted average steady-state PC values before and after insulin addition against their respective Δt intervals (Fig. 3D). At each Δt *v*alue, the steady-state PC level after insulin is always higher than its "before-insulin" counterpart, indicating less-mobile GLUT4 structures, consistent with results shown in Fig. 3A and B and visual inspection of Movie S1 in the supplemental material. Fitting the data with a two-exponential decay model (lines in Fig. 3D) (see Fig. S2 in the supplemental material for detail) reveals a population of immobile GLUT4 structures, whose temporal colocalization is insensitive to increasing Δt values (i.e., residual PC when Δt approaches infinity). Importantly, insulin greatly enlarges this pool of immobile GLUT4 structures (i.e., ~2.5-fold increase in residual PC) for the cell shown in Fig. 3 and for six adipocytes studied (i.e., ~1.5-fold increase in residual PC [see Fig. S2 in the supplemental material]).

Insulin stimulation results in rapid accumulation of GLUT4 molecules in immobile clathrin-coated pits. Taken together, the results of the above analyses show that insulin treatment of cultured adipocytes leads to immobilization of GLUT4 in punctate structures in the TIRF zone. This confirms the observations of Lizunov et al. (30), who also noted this phenomenon. These workers proposed that this immobilization of GLUT4 reflects the tethering of GLUT4 vesicles with the PM prior to fusion. An alternative possibility is that after membrane fusion, GLUT4 moves to localized regions within the PM which are relatively immobile. The latter hypothesis is supported by recently published work, which characterized a large population of immobile clathrin-coated patches in primary adipocytes and COS cells using an EGFP-tagged clathrin light chain construct (clathrin-EGFP) (2). These findings are consistent with previous imaging results indicating 70 to 80% of clathrin-coated pits are static (34). However, photobleaching studies and TIRF imaging at 50 fps carried out by Bellve et al. indicate that these seemingly "static" clathrin patches are active sites for transferrin receptor endocytosis (2).

To test this hypothesis, 3T3-L1 adipocytes were cotransfected with GLUT4-EGFP and a precharacterized dsRed-tagged clathrin light chain construct (i.e., clathrin-dsRed) (32), and two-color TIRF microscopy was carried out as described in the Fig. 4 legend. Movie S3 in the supplemental material shows a dramatic insulin-stimulated increase of GLUT4-EGFP fluorescence in the TIRF evanescence field, which is accompanied by extensive membrane ruffling events. In contrast, the clathrin-dsRed signal is modestly enhanced upon insulin stimulation and the majority of clathrin-coated pits appear to be immobile throughout the experiment (see Movie S4 in the supplemental material). Average results from five cells indicate that insulin increases the clathrin-dsRed fluorescence in the TIRF evanescence field by only ~15% (data not shown), which is significantly smaller than the correspondent ~300% increase of GLUT4-EGFP fluorescence shown in Fig. 2D. Since the clathrin-coated pits are mostly localized to the inner leaflet of the PM, this result indicates that insulin induces no or little change in PM proximity to the glass-water interface, which cannot account for the significant increase in the GLUT4-EGFP fluorescence in the evanescence field (Fig. 2D). Representative colocalization images acquired before and after insulin addition are shown in Fig. 4A and D, respectively. Under basal conditions, GLUT4 (green) and clathrin (red) compartments have limited colocalization (white) (Fig. 4A). Ten minutes after insulin addition, GLUT4-EGFP fluorescence increases dramatically, and essentially all clathrin-coated pits turn white, suggesting GLUT4-EGFP occupancy (Fig. 4D). To show the colocalization details, a segment of the cell (box in Fig. 4A or D) is magnified and shown in Fig. 4B and C (before insulin) and Fig. 4E and F (10 min of insulin). For the two clathrin images taken 15 min apart, the overall clathrin distribution pattern remains essentially unchanged (Fig. 4C and F) except for a small lateral shift caused by insulin addition. Before insulin, there is little GLUT4-EGFP presence in the clathrin-coated pits (Fig. 4B), which are all filled with GLUT4-EGFP after 10 min of insulin stimulation (Fig. 4E). This result indicates that insulin-induced immobilization of punctate GLUT4 structures (Fig. 3; also see Fig. S2 in the supplemental material) can be largely attributed to GLUT4 accumulation in "static" clathrin-coated pits.

To quantify temporal changes of GLUT4-clathrin colocalization, we created binary images of GLUT4 and clathrin compartments (see Fig. S3 in the supplemental material) using algorithms demonstrated in Fig. S1 in the supplemental material. Colocalization of two binary clathrin images acquired under the basal conditions and separated by 1 min indicates that the majority of the clathrin compartments have limited lateral mobility (see Fig. S4F in the supplemental material), which is consistent with visual inspection of Movie S4 in the supple-

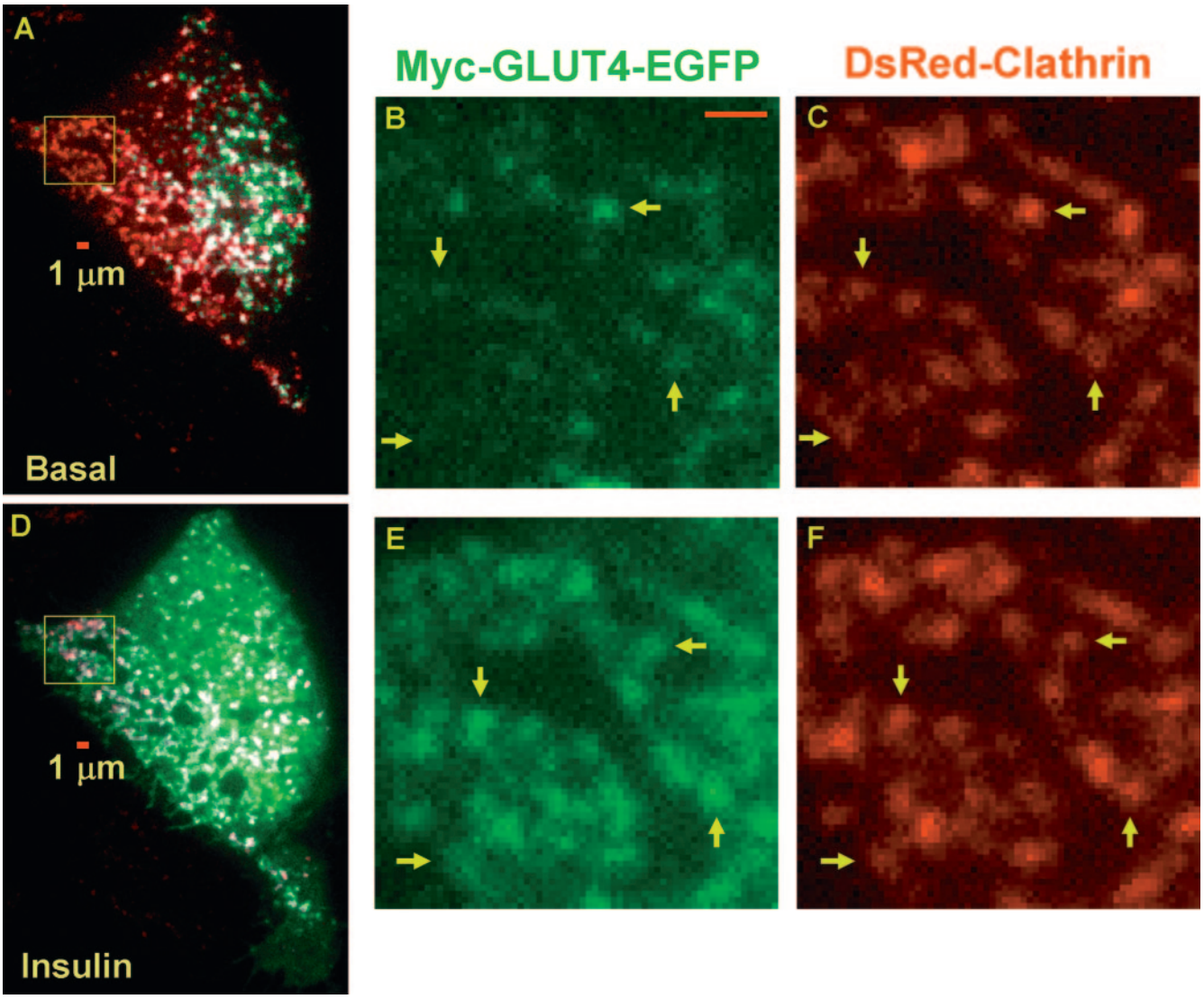

FIG. 4. Insulin promotes GLUT4 accumulation in clathrin-coated membranes. Two-color TIRF microscopy of adipocytes coexpressing GLUT4-EGFP and clathrin-dsRed was carried out under the basal conditions for 5 min, followed by 100 nM insulin stimulation for 15 min. One GLUT4-EGFP image and one clathrin-dsRed image were acquired every 2 s with a 200-ms interval between the green and red images. Thus, a total of 1,200 TIRF images can be split into individual GLUT4 (see Movie S3 in the supplemental material) and clathrin (see Movie S4 in the supplemental material) movies, each containing 600 images acquired at one frame per 2 s. Representative colocalization (white) between GLUT4 (green) and clathrin (red) compartments acquired before or 10 min after insulin stimulation are shown in images A and D, respectively. Magnified views of the boxed regions (64 by 64 pixels) in images A and D are shown in images B and C and images E and F, respectively. Although images C and F were taken 15 min apart, the same pattern of clathrin distribution, although laterally shifted, is still distinguishable (e.g., arrows in C and F). In contrast, GLUT4 occupancy of these clathrin-coated membranes increases dramatically after insulin stimulation (compare B and E). Scale bars in images A, B, and D are 1 μm.

mental material. Interestingly, colocalization of the correspondent binary GLUT4 images also reveals a population of immobile GLUT4 structures even in the quiescent cell (see Fig. S4C in the supplemental material), which is consistent with the immobile fraction of GLUT4 structures in quiescent cells revealed by Fig. 3D (also see Fig. S2 in the supplemental material). Importantly, the majority of these immobile GLUT4 structures in the unstimulated state have already colocalized with clathrin (white arrows in Fig. S4C and F in the supplemental material), likely reflecting basal GLUT4 endocytosis.

Representative colocalization between binary GLUT4 and clathrin images is shown in Fig. 5A (before insulin) and B (10 min after insulin). In the quiescent cell, there was partial overlap between GLUT4 and clathrin compartments (Fig. 5A). Ten minutes after insulin addition, essentially all clathrin-coated pits were occupied by GLUT4, although not all GLUT4 vesicles were colocalized with clathrin (Fig. 5B). Thus, we calculated percentages of clathrin pixels colocalizing with GLUT4 pixels for 600 pairs of TIRF images obtained from each experiment. These numbers were further corrected for random colocalization (see Materials and Methods) and plotted in Fig. 5C, which clearly shows an insulin-stimulated occupancy of

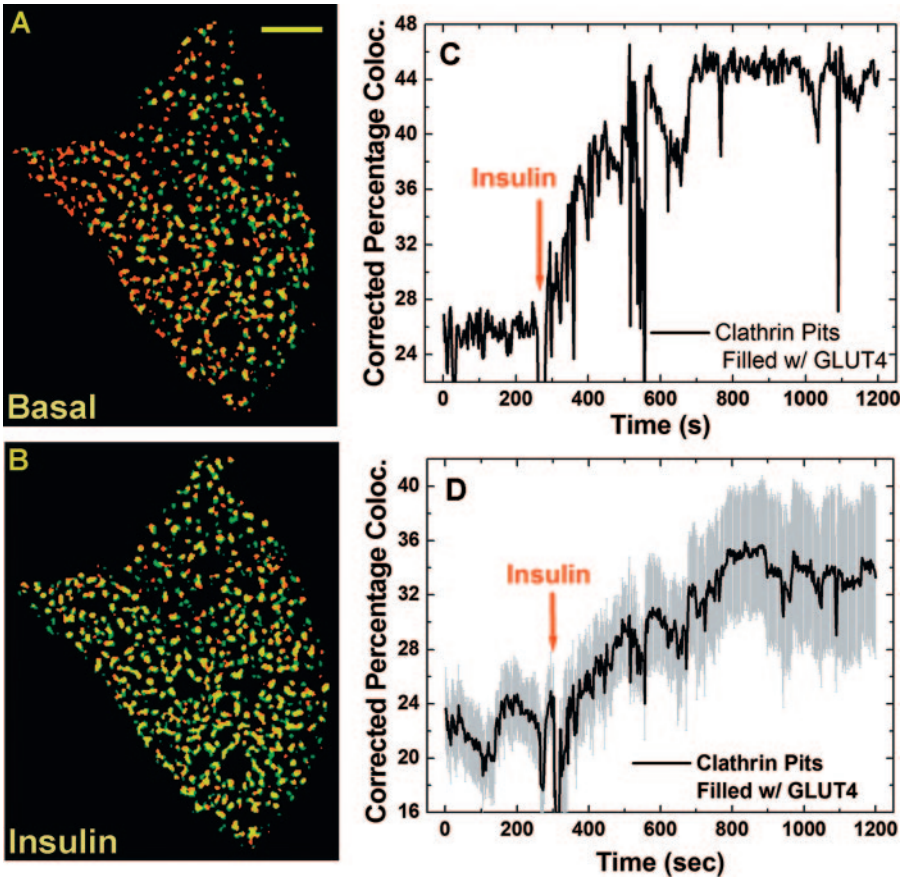

FIG. 5. Quantification of insulin-stimulated GLUT4 accumulation in clathrin-coated membranes. Binary images containing the punctate GLUT4 or clathrin structures (see Fig. S3 in the supplemental material) were prepared using algorithms demonstrated in Fig. S1 in the supplemental material. Representative colocalization (yellow) images between pairs of binary GLUT4 (green) and clathrin (red) images are shown in A and B for the basal and 10-min insulin stimulation conditions, respectively. Scale bar in A is 5 μm. For the entire image sequence (i.e., 600 pairs of GLUT4 and clathrin images; see Movies S3 and S4 in the supplemental material), the percentages of clathrin pixels colocalizing with corresponding GLUT4 pixels, corrected for random colocalization (see Materials and Methods), are shown in panel C (i.e., spatial clathrin-GLUT4 colocalization). Fluctuations in the colocalization curve (e.g., between ~500 s and ~550 s) are due to focus drifts in the TIRF images (see corresponding time windows in Movies S3 and S4 in the supplemental material) but not due to dramatic changes in clathrin-GLUT4 colocalization. The average values of the clathrin-GLUT4 colocalization kinetics are shown in panel D with associated standard errors of the mean (gray shading).

clathrin-based endocytic structures by GLUT4 molecules. An average result from six cells indicates insulin increases the percentage of clathrin pixels colocalized with GLUT4 by ~1.5-fold (i.e., corrected PC value increases from ~22% to ~34%; Fig. 5D), which corresponds to the ~1.5-fold increase in the immobilized GLUT4-containing pixels in the TIRF evanescence field after insulin stimulation (see Fig. S2 in the supplemental material). To control for the potential detrimental effect of dsRed tagging of clathrin light chain, an mRFP1-tagged GLUT4 construct was created (GLUT4-mRFP1 [see Materials and Methods]), and a similar two-color TIRF study (see above) was carried out using 3T3-L1 adipocytes transiently coexpressing clathrin-EGFP (2) and clathrin-mRFP1. Similar increases in GLUT4-clathrin colocalization are detected (see Fig. S4 in the supplemental material). Thus, combined evidence (see above) indicates that insulin-induced accumulation of GLUT4 molecules in immobile clathrin-coated patches largely accounts for the apparent immobilization of punctate GLUT4 structures observed at the temporal resolution of 1 fps (Fig. 3; also see Fig. S2 in the supplemental material).

Single GLUT4 vesicles dock and fuse with the PM. To test whether enhanced exocytic vesicle tethering/docking at the PM can contribute to the observed insulin immobilization of punctate GLUT4 structures, as previously suggested (30), we carried out TIRF imaging at a higher temporal resolution (10 fps; see illustration in Fig. 8) to detect single-vesicle docking/fusion events. At this increased temporal resolution, abundant fusion events were detected in insulin-stimulated adipocytes (Fig. 6; also see Movie S10 in the supplemental material). In contrast, previous TIRF studies using cultured and primary adipocytes did not address exocytic GLUT4 vesicle fusion (41) or detected too few fusion events for statistical characterization (28, 30). In agreement with findings of TIRF studies of various types of exocytic events in different cell lines (38, 48, 33), single-vesicle fusion was manifested as a punctate GLUT4-EGFP signal spreading out in the TIRF evanescence field in a "puff," which was typically completed within 1 s (Fig. 6C) (see Movie S7 in the supplemental material). Quantitatively, peak vesicle intensity (i.e., I_P; highest pixel intensity of the exocytic vesicle) dropped to background levels during the fusion process (Fig.

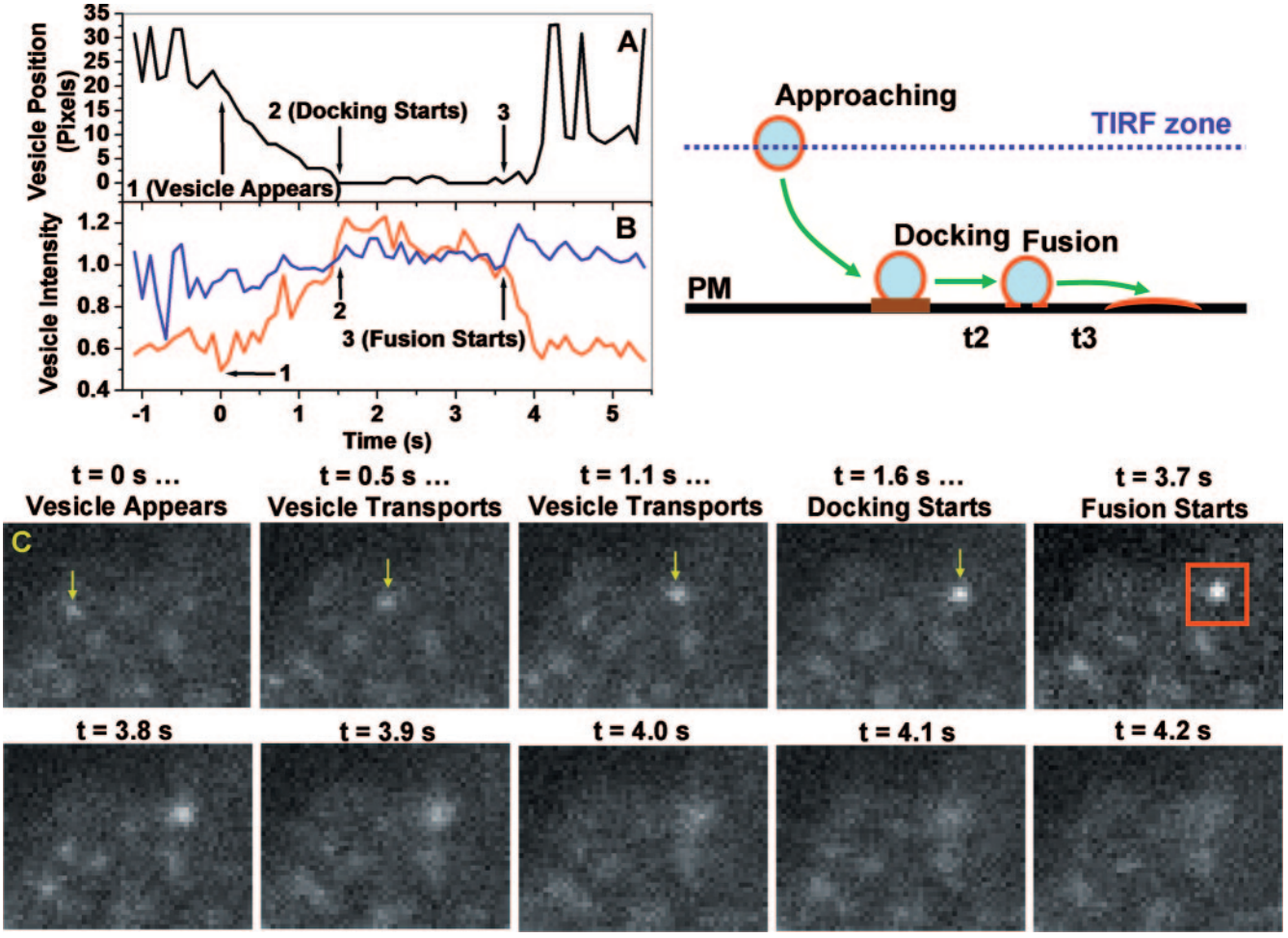

FIG. 6. Kinetics of single GLUT4 vesicle docking and fusion with the PM. TIRF imaging at 10 fps of 3T3-L1 adipocytes transiently expressing GLUT4-EGFP was carried out using a burst protocol, illustrated in Fig. 8. For each fusion event, three parameters are obtained: peak vesicle intensity (I_P; see the text), total vesicle intensity (I_V), and vesicle position (P_V). The I_P (red line) and I_V intensities (blue line) are normalized to their respective values obtained at the fusion time (i.e., arrow 3 in panels A and B; red box in panel C) and are plotted in panel B. Assigning vesicle position 0 at the fusion site (i.e., arrow 3 in panel A), vesicle distances to the fusion site are computed and plotted in panel A. Critical stages of the docking/fusion process (i.e., vesicle appears, docking starts, and fusion starts) are indicated by arrows in panels A and B, and representative images are shown in panel C. The cartoon illustrates distinct stages of single-vesicle transport, docking, and fusion.

6B). In contrast, total vesicle intensity (i.e., I_V; total pixel intensity within a 1.3- by 1.3-μm box centered at I_P [Fig. 6C]) initially increased upon fusion (Fig. 6B), reflecting GLUT4-EGFP molecules diffusing into the PM, which was located at a stronger TIRF evanescence field (see illustration in Fig. 6). Using these criteria, dozens of fusion events were visually identified in insulin-stimulated adipocytes in our experiments. Significantly, such fusion events, although less frequent, were also detected in the same cell before insulin addition (e.g., see Movie S8 in the supplemental material). Importantly, all fusion events appeared to be preceded by a vesicle tethering/docking period (i.e., I_P positions prior to vesicle fusion do not deviate >2 pixels [100 nm/pixel] from the fusion site [Fig. 6C]) that typically lasted a few seconds (Fig. 6A). In the example shown in Fig. 6, the entire translocation process, starting from a GLUT4 vesicle entering (t = 0 s) the TIRF evanescence field to its docking on the PM (t = 1.6 s), is observed (Fig. 6A and C) and is accompanied by increasing I_P intensities (Fig. 6B) as the vesicle descends towards stronger TIRF illumination (illustration in Fig. 6). In another case, a GLUT4-containing vesicle quickly (within 0.1 s) appeared in the TIRF evanescence field and immediately tethered/docked to the PM; vesicle fusion then occurred after the obligatory docking period (e.g., see Fig. S5 in the supplemental material).

Development of Fusion Assistant for statistical characterization of exocytic GLUT4 vesicle docking/fusion. Manual identification and characterization of single-vesicle fusion events (Fig. 6) (see Fig. S5 in the supplemental material) among thousands of TIRF images are inefficient, incomplete, and potentially biased. Thus, we developed a computer program (Fusion Assistant) that automatically screens all TIRF images and identifies candidate fusion events for further visual confirmation. Briefly, Fusion Assistant first computes all potential trajectories of single-vesicle movements in the TIRF evanescence field (see Materials and Methods). These trajectories are first screened for possible single-vesicle fusion using

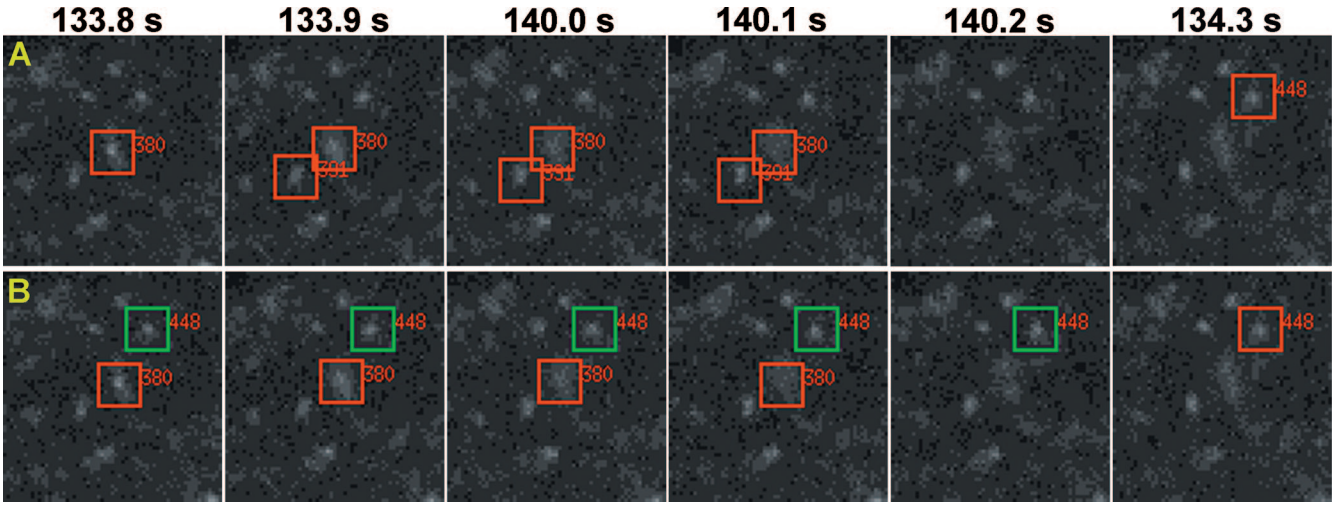

FIG. 7. Fusion Assistant. We have developed a computer program (i.e., Fusion Assistant) that assists the identification and characterization of single-vesicle docking/fusion kinetics. For example, Fusion Assistant identifies three candidate fusion events starting at 133.8 s, 133.9 s, or 134.3 s after insulin addition (A). These potential fusion events are numbered (380, 391, and 448) and are continuously highlighted with red boxes (1.3 by 1.3 μm) for visual confirmation. For fusion event 448, only the start of the fusion at 134.3 s is shown. Two fusion events (380 and 448) are confirmed and highlighted with red boxes (B). Docked vesicle positions are highlighted with green boxes (examples shown for fusion 448 in B only). All candidate fusion events identified by Fusion Assistant in the last minutes of insulin stimulation (see burst protocol in Fig. 8) are shown in Movie S9 in the supplemental material, and those visually confirmed and their associated docked vesicle positions are shown in Movie S10 in the supplemental material.

two rules derived from characterization of dozens of manually selected fusion events: (i) upon fusion, the total vesicle intensity (I_V) has to increase by >10% within 1 s, while (ii) the peak vesicle intensity (I_P) has to decrease by >50% during the same 1-s time window. Thus, a potential fusion time (T_F) is identified as the time when I_V starts its >10% increase, while simultaneously (within ± 0.2 s) I_P also starts its >50% decrease (Fig. 6B; also see Fig. S5B in the supplemental material). These potential fusion events are further selected by rule 3, that tracking back from the fusion site at T_F, the prior vesicle positions (P_V) have to be stationary (i.e., do not deviate from the fusion site by >2 pixels) for ≥1 s. Finally, all potential fusion events are numbered and highlighted by red boxes during vesicle fusion and are presented in an interactive display on the computer screen for further visual confirmation (Fig. 7A; also see Movie S9 in the supplemental material).

Actual fusion events are confirmed by visual inspection that (i) the candidate vesicle indeed disappears, while (ii) its punctate GLUT4-EGFP signal characteristically spreads out in a "puff" in the TIRF evanescence field (e.g., see Movies S7 and S8 in the supplemental material). Thus, the use of Fusion Assistant combined with visual confirmation reproducibly identifies fusion events we found manually, plus two- to threefold more events that we initially missed by manual inspection (e.g., see Fig. 7B; also see Movie S10 in the supplemental material). Furthermore, once a fusion site (i.e., pixel coordinates of I_P at T_F) is identified, Fusion Assistant views previous TIRF images to define the vesicle docking duration. In this case, the vesicle is considered to be tethered/docked if the pixel positions associated with the preceding I_P values do not deviate out of a circle of 2-pixel radius centered at the fusion site (Fig. 6A; also see Fig. S5A in the supplemental material). These docked vesicles identified by Fusion Assistant are highlighted with green boxes and displayed on the computer screen for further visual confirmation (Fig. 7B; also see Movie S10 in the supplemental material). The development of Fusion Assistant greatly speeds up identification and characterization of single-vesicle docking/fusion kinetics, so that manual screening and characterization for an entire day can be matched by the computer-assisted procedures in a few hours.

Insulin increases the fusion frequency of exocytic GLUT4 vesicles while decreasing the docking duration prior to vesicle fusion. Using the above novel capabilities, docking and fusion kinetics of hundreds of exocytic GLUT4 vesicles were resolved, enabling statistical examination of its potential insulin regulation (Fig. 8). This analysis revealed that insulin gradually increases the exocytic fusion rate, which appears to reach a maximum level a few minutes after insulin addition (Fig. 8A). This maximum fusion rate is ~4 times higher than that detected in basal adipocytes (Fig. 8A), which, combined with a two- to threefold inhibition of the GLUT4 endocytosis rate by insulin (45, 47), could account for the 5- to 10-fold increase in PM GLUT4 concentration following insulin stimulation (4, 46, 14).

The size of GLUT4 vesicles in 3T3-L1 adipocytes (i.e., 30 to 200 nm [31]) is below the measured lateral resolution of our TIRF microscope (i.e., 259 nm), which could cause an underestimation of the number of fusion events. Thus, only a fusion event of a GLUT4 vesicle with sufficient brightness and spatial separation from its neighbors (vesicle-to-vesicle distance of >259 nm) is reliably detected. However, the ~4-fold insulin-stimulated increase in the fusion frequency (Fig. 8A) and the apparent time dependency of that increase (probably reflecting insulin mobilization of intracellular GLUT4 vesicles towards the PM) suggest that a representative population of total fusion events is selected in our analysis. Thus, we examined statistical distributions of vesicle tethering/docking durations for fusion events occurring before and after insulin stimulation of the same adipocytes (Fig. 8B). We have initially focused on

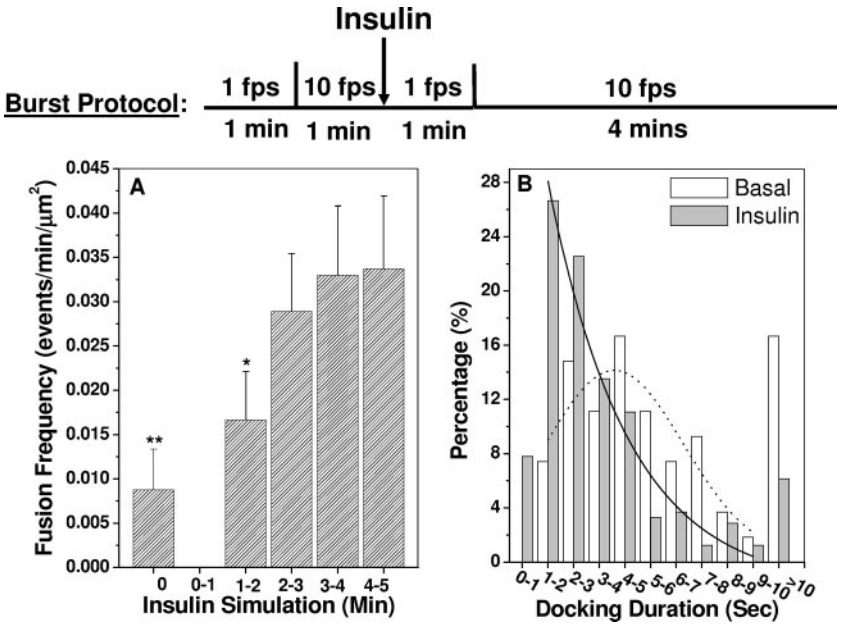

FIG. 8. Insulin increases the fusion frequency of exocytic GLUT4 vesicles and decreases docking duration prior to vesicle fusion. Burst protocol: periods of 1 min of imaging at 1 fps are used to establish imaging focus for subsequent burst imaging at 10 fps (see illustration). Fusion Assistant combined with visual confirmation (Fig. 7) identified 54 fusion events in 6 quiescent adipocytes and 244 fusion events in 3 insulin-stimulated cells. Fusion frequencies (fusion events per min per μm^2 of coverslip-attached PM) for each minute of the burst imaging are plotted in panel A, together with associated standard errors of the mean. The fusion frequencies obtained before insulin addition and during the 1- to 2-min period of insulin stimulation are different from that obtained at the 4- to 5-min period of insulin stimulation at confidence levels of 99% (**) and 90% (*), respectively. Distributions of vesicle docking durations for fusion events before (white bars) and after (gray bars) insulin addition are plotted in panel B. Solid and dotted lines are nonlinear least-square fits of the data (between 1 and 10 s) using Poisson and Gaussian distribution models, respectively.

fusion events with docking durations of ≥1 s (see rule 3 above), because Fusion Assistant currently produces too many false positives if the prefusion docking duration is set to be <1 s. In quiescent cells, the tethering/docking durations are mostly distributed within 1 to 8 s (Fig. 8B), which can be loosely fitted to a Gaussian distribution. Insulin dramatically shifted this distribution to short times (Fig. 8B), and the manual verification procedure following use of Fusion Assistant (see above) also discovered a population (underestimated with our current selection rule 3) of fusion events with docking durations of <1 s. The presence of GLUT4 vesicles with short tethering/docking durations, however, was predicted by the Poisson distribution fit of the "after-insulin" tethering/docking durations. Furthermore, there was a >2-fold increase of fusion events with tethering/docking durations of >10 s in quiescent cells compared to those in stimulated cells (Fig. 8B). Overall, these results represent the first direct evidence in live adipocytes indicating insulin regulation of the process of exocytic GLUT4 vesicle tethering/docking with the PM.

DISCUSSION

Although it has been observed more than two and a half decades ago that insulin mobilizes intracellular GLUT4 vesicles towards the adipocyte cell surface to enhance glucose uptake, the detailed molecular mechanisms of this complicated trafficking process are still largely unknown (7, 43). In addition to movements of intracellular GLUT4-containing vesicles towards the PM, it has been suggested that exocytic GLUT4 vesicle tethering/docking/fusion at the PM is also a critical step regulated by insulin (11, 22, 20, 37). Recently in vitro membrane reconstitution experiments demonstrated that insulin enhances GLUT4-containing vesicle fusion to a PM fraction by ~9-fold, which is dependent on Akt recruitment to the insulin-activated PM fraction (27). This is supported by evidence that Akt activity is essential to overcome a low-temperature block of exocytic GLUT4 vesicle fusion with the PM but not required for intracellular GLUT4 exocytosis to the cell surface vicinity (42). Nevertheless, the opposite conclusion was derived from a recent quantitative TIRF study, which suggested that Akt activity is required only for intracellular recruitment of GLUT4 vesicles to the PM region (13). The latter study also indicated insulin-stimulated phosphatidylinositide 3-phosphate kinase activity is apparently indispensable for the vesicle fusion process, but through an Akt-independent mechanism (13). This concept is in agreement with results of experiments showing addition of the phosphatidylinositide 3-phosphate kinase product, phosphatidylinositide-3,4,5-triphosphate, to insulin-sensitive muscle cells increases exocytic GLUT4 vesicle fusion with the PM (21). Thus, direct analysis of the kinetics of GLUT4 vesicle docking/fusion in intact cells is required to rigorously examine possible regulation of these processes by insulin.

The present study employs TIRF microscopy as a powerful tool (1) to dissect single-vesicle docking/fusion processes at the adipocyte PM, where the proximal insulin signaling intermediates localize to potentially regulate GLUT4 vesicle fusion and then endocytosis. While valuable insights about GLUT4

trafficking have been gained from previous TIRF studies quantifying overall GLUT4-EGFP signals in the evanescence field (13, 41), the feasibility of analyzing single GLUT4-containing vesicle docking/fusion events is only recently demonstrated (30). However, substantial technical difficulties still exist, because the reported physical sizes of the GLUT4 vesicles are below the optical resolution of TIRF microscopy (31). Thus, we developed unbiased and quantitative tools (e.g., Fusion Assistant) to analyze thousands of TIRF images so that statistically valid conclusions can be derived. Using this system, we show here that insulin signaling causes changes in the kinetics of GLUT4-containing vesicle tethering/docking with the PM. Specifically, we find that insulin treatment of cultured adipocytes decreases the duration between vesicle tethering/docking and vesicle fusion with the PM (Fig. 6 to 8). The rate at which GLUT4 apparently diffuses away from the fusion sites (i.e., 0.9 ± 0.1 s) does not appear to be altered by insulin action in our studies. Thus, the data presented here indicate that one or more cellular components required for the transition from docking of GLUT4-containing vesicles to their fusion is a target of insulin signaling.

A second advance made in the present studies is the understanding of the cellular basis for the apparent insulin-induced immobilization of GLUT4-containing structures in the TIRF zone, as originally observed by Lisunov et al. (30). Using the novel temporal colocalization method (Fig. 3; also see Fig. S1 and S2 and Movie S2 in the supplemental material), we first confirmed their previous analysis (30) that insulin causes a dramatic apparent immobilization of GLUT4-containing structures in the evanescence field. We then used the two-color TIRF microscope to provide the technology to colocalize GLUT4-EGFP with other PM structures. Using this approach, we discovered that following insulin stimulation of cultured adipocytes, GLUT4-EGFP increasingly localizes with immobile clathrin-coated patches (Fig. 4 and 5; also see Fig. S3 and S4 and Movies S3, S4, S5, and S6 in the supplemental material). This contrasts with the interpretation of Lizunov et al. (30) that these GLUT4-containing structures are related to exocytic GLUT4 vesicle tethering/docking to the PM. Our conclusion is further supported by the published work of our colleagues using the same TIRF microscope, which shows that clathrin-coated patches on the adipocyte PM appear to be immobile for more than 30 min (2). However, at a higher temporal resolution of 50 fps, these apparently "static" clathrin patches are undergoing rapid remodeling necessary for transferrin receptor endocytosis (2). Taken together, the data described above (Fig. 3 to 5) support the hypothesis that following insulin stimulation of GLUT4 translocation and fusion with the PM, GLUT4 molecules diffuse away from the fusion sites and are trapped in clathrin-coated structures that mediate its endocytosis. These data are not incompatible with the idea that other endocytosis pathways are also used to internalize GLUT4, as recently suggested (3) (see below).

It should be noted that during the revision of the manuscript, an independent TIRF analysis of GLUT4-containing vesicle docking/fusion kinetics was published (1), which reached the same conclusion as ours that insulin reduces the tethering/docking duration prior to membrane fusion (Fig. 8). However, while our studies focus on the limited population of docked vesicles successfully proceeding to membrane fusion, Bai et al. (1) included an analysis of "docked" vesicles that subsequently leave the TIRF evanescence field. In our view, a vesicle that becomes immobilized and then shows transient fluorescence enhancement does not necessarily signify a docked vesicle. This is because the limited resolution of light microscopy does not allow defining the position of the vesicle as docked against the PM. Nevertheless, we (Fig. 8A) and Bai et al. (1) have determined that insulin stimulates exocytic GLUT4 vesicle fusion by four- and eightfold at 35°C and 30°C, using our respective methods. In addition, both studies estimate the typical tethering/docking duration to last less than a few seconds, instead of the minutes of duration suggested by the immobilized GLUT4 structures in the studies of Lizunov et al. (30). The apparent GLUT4 diffusion from fusion sites into the PM (i.e., punctate GLUT4 fluorescence spreading out in the TIRF evanescence field until its I_P value reaches the background level [Fig. 6B and C; also see Movies S7, S8, and S10 in the supplemental material]) takes 0.9 ± 0.1 s, which is unchanged by insulin in our study (data not shown). This also contrasts to the model suggested by Lizunov et al., in which GLUT4 molecules are slowly (>20 s) released from fusion sites into the PM (30). However, our estimated GLUT4 diffusion rate in the PM (e.g., estimated from the rate of GLUT4-EGFP fluorescence spreading in the 1.3- by 1.3-μm box in Fig. 6C) is 1.2×10^{-9} cm^2/s, which is in excellent agreement with the correspondent rates of 1.4×10^{-9} cm^2/s and 0.93×10^{-9} cm^2/s measured by Lizunov et al. (30) and Bai et al. (1), respectively.

It is important to point out that none of the TIRF studies to date, including ours, are able to distinguish between vesicle tethering and vesicle docking, which are proposed to be mediated by the exocyst and SNARE complexes, respectively (8, 20, 40). Furthermore, the SNARE core formation among syntaxin 4, synaptosome-associated protein 23, and vesicle-associated membrane protein 2 is regulated by SNARE-associated proteins (e.g., Munc18, tomosyn, and syndet) (43), which likely constitutes the molecular basis for insulin regulation of GLUT4 vesicle docking to the PM. Thus, further understanding of the tethering/docking/fusion processes requires identification of the underlying molecular machines that can be examined by two-color TIRF microscopy in relationship to GLUT4 trafficking. The additional color channel provides a valuable molecular context for interpreting the interplay of specific GLUT4 trafficking events with specific cellular components, as we demonstrated for the insulin-induced immobilization of GLUT4 within static clathrin-based structures (Fig. 4 and 5).

Recently it was reported that the internalization of GLUT4 occurs by two distinct pathways, one involving the classic clathrin-mediated endocytosis route discussed in this paper and the other involving a cholesterol-dependent/clathrin-independent process that is less well described (3). Interestingly, the latter pathway appears to dominate in the basal state. However, insulin inhibits this cholesterol-dependent internalization pathway and thus inhibits the rate of overall GLUT4 internalization, as previously reported (10, 43). A consequence of this insulin action is that GLUT4 internalization is virtually entirely mediated by the clathrin-dependent pathway in stimulated cells (3). Thus, our results showing a significant increase in the cell surface GLUT4 associated with clathrin patches following

insulin stimulation (Fig. 4 and 5) (see Fig. S3 and S4 in the supplemental material) provide direct visual support for this model of GLUT4 endocytosis (3). The fact that GLUT4 appears to accumulate at high concentrations at these sites also raises the possibility that its internalization through this clathrin-dependent pathway slows in the stimulated state, but this idea will have to be rigorously tested. Nonetheless, the original result and suggestion (10) that insulin's action to inhibit GLUT4 internalization may contribute significantly to the overall increase in cell surface GLUT4 is now well supported (3, 43).

Based on the above considerations and results from many laboratories, it appears that insulin signaling molecules interface with the GLUT4 trafficking pathway at several sites and steps. The cumulative effects of these multiple modulations are a large increase in cell surface GLUT4. These insulin-sensitive steps include movements of GLUT4-containing vesicles from below the TIRF zone into the TIRF zone (13), the tethering and docking of GLUT4-containing vesicles with the PM (1, 20; this report), and GLUT4 internalization (10). Additionally, insulin also exerts a smaller effect on the exocytosis of vesicles that transport transferrin receptor to the cell surface (46). These vesicles derive from the conventional recycling pathway and appear to be different from the vesicles highly enriched in GLUT4 (7). Other sites of insulin action on the overall recycling pathway for GLUT4 may also exist. Some of these steps in the GLUT4 trafficking pathway appear to involve motor proteins and both the microtubule- and actin-based cytoskeleton (5, 19, 39). Indeed, our laboratory (39) and Lizunov et al. (30) reported direct microscopic evidence in live adipocytes for GLUT4-containing vesicles moving on microtubules. Recent work from our laboratory also identified the unconventional myosin Myo1c as a required component of optimal insulin-stimulated GLUT4 translocation to the PM (5). These results suggested Myo1c may act close to or at the fusion step of GLUT4 trafficking (6). Thus, the data presented here and by Bai et al. (1) indicating that insulin action modulates the kinetics of the tethering/docking step raise the possibility that Myo1c may be involved in this action. Future studies designed to test this idea and to identify the components involved in this action of insulin will be a major challenge for the field.

ACKNOWLEDGMENT

This work was supported by National Institutes of Health Program Project grant P01 DK60564.

REFERENCES

1. **Bai, L., Y. Wang, J. Fan, Y. Chen, W. Ji, A. Qu, P. Xu, D. E. James, and T. Xu.** 2007. Dissecting multiple steps of GLUT4 trafficking and identifying the sites of insulin action. Cell Metab. **5:**47–57.
2. **Bellve, K. D., D. Leonard, C. Standley, L. M. Lifshitz, R. A. Tuft, A. Hayakawa, S. Corvera, and K. E. Fogarty.** 2006. Plasma membrane domains specialized for clathrin-mediated endocytosis in primary cells. J. Biol. Chem. **281:**16139–16146.
3. **Blot, V., and T. E. McGraw.** 2006. GLUT4 is internalized by a cholesterol-dependent nystatin-sensitive mechanism inhibited by insulin. EMBO J. **25:** 5648–5658.
4. **Bogan, J. S., A. E. McKee, and H. F. Lodish.** 2001. Insulin-responsive compartments containing GLUT4 in 3T3-L1 and CHO cells: regulation by amino acid concentrations. Mol. Cell. Biol. **21:**4785–4806.
5. **Bose, A., A. Guilherme, S. I. Robida, S. M. Nicoloro, Q. L. Zhou, Z. Y. Jiang, D. P. Pomerleau, and M. P. Czech.** 2002. Glucose transporter recycling in response to insulin is facilitated by myosin Myo1c. Nature **420:**821–824.
6. **Bose, A., S. Robida, P. S. Furcinitti, A. Chawla, K. Fogarty, S. Corvera, and M. P. Czech.** 2004. Unconventional myosin Myo1c promotes membrane fusion in a regulated exocytic pathway. Mol. Cell. Biol. **24:**5447–5458.
7. **Bryant, N. J., R. Govers, and D. E. James.** 2002. Regulated transport of the glucose transporter GLUT4. Nat. Rev. Mol. Cell Biol. **3:**267–277.
8. **Chen, Y. A., and R. H. Scheller.** 2001. SNARE-mediated membrane fusion. Nat. Rev. Mol. Cell Biol. **2:**98–106.
9. **Cormen, T. H., C. E. Leiserson, and R. L. Rivest.** 1990. Introduction to algorithms. The MIT Press, Cambridge, MA.
10. **Czech, M. P., and J. M. Buxton.** 1993. Insulin action on the internalization of the GLUT4 glucose transporter in isolated rat adipocytes. J. Biol. Chem. **268:**9187–9190.
11. **Elmendorf, J. S., D. J. Boeglin, and J. E. Pessin.** 1999. Temporal separation of insulin-stimulated GLUT4/IRAP vesicle plasma membrane docking and fusion in 3T3L1 adipocytes. J. Biol. Chem. **274:**37357–37361.
12. **Foster, L. J., and A. Klip.** 2000. Mechanism and regulation of GLUT-4 vesicle fusion in muscle and fat cells. Am. J. Physiol. Cell Physiol. **279:**C877–C890.
13. **Gonzalez, E., and T. E. McGraw.** 2006. Insulin signaling diverges into Akt-dependent and -independent signals to regulate the recruitment/docking and the fusion of GLUT4 vesicles to the plasma membrane. Mol. Biol. Cell **17:**4484–4493.
14. **Govers, R., A. C. Coster, and D. E. James.** 2004. Insulin increases cell surface GLUT4 levels by dose dependently discharging GLUT4 into a cell surface recycling pathway. Mol. Cell. Biol. **24:**6456–6466.
15. **Guilherme, A., N. A. Soriano, S. Bose, J. Holik, A. Bose, D. P. Pomerleau, P. Furcinitti, J. Leszyk, S. Corvera, and M. P. Czech.** 2004. EHD2 and the novel EH domain binding protein EHBP1 couple endocytosis to the actin cytoskeleton. J. Biol. Chem. **279:**10593–10605.
16. **Hashiramoto, M., and D. E. James.** 2000. Characterization of insulin-responsive GLUT4 storage vesicles isolated from 3T3-L1 adipocytes. Mol. Cell. Biol. **20:**416–427.
17. **Huang, J., T. Imamura, and J. M. Olefsky.** 2001. Insulin can regulate GLUT4 internalization by signaling to Rab5 and the motor protein dynein. Proc. Natl. Acad. Sci. USA **98:**13084–13089.
18. **Huang, S., L. Lifshitz, V. Patki-Kamath, R. Tuft, K. Fogarty, and M. P. Czech.** 2004. Phosphatidylinositol-4,5-bisphosphate-rich plasma membrane patches organize active zones of endocytosis and ruffling in cultured adipocytes. Mol. Cell. Biol. **24:**9102–9123.
19. **Imamura, T., J. Huang, I. Usui, H. Satoh, J. Bever, and J. M. Olefsky.** 2003. Insulin-induced GLUT4 translocation involves protein kinase C-lambda-mediated functional coupling between Rab4 and the motor protein kinesin. Mol. Cell. Biol. **23:**4892–4900.
20. **Inoue, M., L. Chang, J. Hwang, S. H. Chiang, and A. R. Saltiel.** 2003. The exocyst complex is required for targeting of Glut4 to the plasma membrane by insulin. Nature **422:**629–633.
21. **Ishiki, M., V. K. Randhawa, V. Poon, L. Jebailey, and A. Klip.** 2005. Insulin regulates the membrane arrival, fusion, and C-terminal unmasking of glucose transporter-4 via distinct phosphoinositides. J. Biol. Chem. **280:**28792–28802.
22. **James, D. E.** 2005. MUNC-ing around with insulin action. J. Clin. Investig. **115:**219–221.
23. **Jiang, Z. Y., A. Chawla, A. Bose, M. Way, and M. P. Czech.** 2002. A phosphatidylinositol 3-kinase-independent insulin signaling pathway to N-WASP/Arp2/3/F-actin required for GLUT4 glucose transporter recycling. J. Biol. Chem. **277:**509–515.
24. **Kandror, K. V.** 2003. A long search for Glut4 activation. Sci. STKE **2003:** PE5.
25. **Kao, A. W., B. P. Ceresa, S. R. Santeler, and J. E. Pessin.** 1998. Expression of a dominant interfering dynamin mutant in 3T3L1 adipocytes inhibits GLUT4 endocytosis without affecting insulin signaling. J. Biol. Chem. **273:** 25450–25457.
26. **Karylowski, O., A. Zeigerer, A. Cohen, and T. E. McGraw.** 2004. GLUT4 is retained by an intracellular cycle of vesicle formation and fusion with endosomes. Mol. Biol. Cell **15:**870–882.
27. **Koumanov, F., B. Jin, J. Yang, and G. D. Holman.** 2005. Insulin signaling meets vesicle traffic of GLUT4 at a plasma-membrane-activated fusion step. Cell Metab. **2:**179–189.
28. **Lampson, M. A., J. Schmoranzer, A. Zeigerer, S. M. Simon, and T. E. McGraw.** 2001. Insulin-regulated release from the endosomal recycling compartment is regulated by budding of specialized vesicles. Mol. Biol. Cell **12:**3489–3501.
29. **Li, L. V., and K. V. Kandror.** 2005. Golgi-localized, gamma-ear-containing, Arf-binding protein adaptors mediate insulin-responsive trafficking of glucose transporter 4 in 3T3-L1 adipocytes. Mol. Endocrinol. **19:**2145–2153.
30. **Lizunov, V. A., H. Matsumoto, J. Zimmerberg, S. W. Cushman, and V. A. Frolov.** 2005. Insulin stimulates the halting, tethering, and fusion of mobile GLUT4 vesicles in rat adipose cells. J. Cell Biol. **169:**481–489.
31. **Martin, S., C. A. Millar, C. T. Lyttle, T. Meerloo, B. J. Marsh, G. W. Gould, and D. E. James.** 2000. Effects of insulin on intracellular GLUT4 vesicles in adipocytes: evidence for a secretory mode of regulation. J. Cell Sci. **113:** 3427–3438.
32. **Merrifield, C. J., M. E. Feldman, L. Wan, and W. Almers.** 2002. Imaging actin and dynamin recruitment during invagination of single clathrin-coated pits. Nat. Cell Biol. **4:**691–698.

33. **Ohara-Imaizumi, M., C. Nishiwaki, T. Kikuta, K. Kumakura, Y. Nakamichi, and S. Nagamatsu.** 2004. Site of docking and fusion of insulin secretory granules in live MIN6 beta cells analyzed by TAT-conjugated anti-syntaxin 1 antibody and total internal reflection fluorescence microscopy. J. Biol. Chem. **279:**8403–8408.
34. **Rappoport, J. Z., S. M. Simon, and A. Benmerah.** 2004. Understanding living clathrin-coated pits. Traffic **5:**327–337.
35. **Robinson, L. J., S. Pang, D. S. Harris, J. Heuser, and D. E. James.** 1992. Translocation of the glucose transporter (GLUT4) to the cell surface in permeabilized 3T3-L1 adipocytes: effects of ATP insulin, and GTP gamma S and localization of GLUT4 to clathrin lattices. J. Cell Biol. **117:**1181–1196.
36. **Sandison, D. R., R. M. Williams, K. S. Wells, J. Strickler, and W. W. Webb.** 1995. Quantitative fluorescence confocal laser scanning microscopy (CLSM), p. 39–53. *In* J. B. Pawley (ed.), Handbook of biological confocal microscopy, 2nd ed. Plenum Press, New York, NY.
37. **Satoh, S., H. Nishimura, A. E. Clark, I. J. Kozka, S. J. Vannucci, I. A. Simpson, M. J. Quon, S. W. Cushman, and G. D. Holman.** 1993. Use of bismannose photolabel to elucidate insulin-regulated GLUT4 subcellular trafficking kinetics in rat adipose cells. Evidence that exocytosis is a critical site of hormone action. J. Biol. Chem. **268:**17820–17829.
38. **Schmoranzer, J., M. Goulian, D. Axelrod, and S. M. Simon.** 2000. Imaging constitutive exocytosis with total internal reflection fluorescence microscopy. J. Cell Biol. **149:**23–32.
39. **Semiz, S., J. G. Park, S. M. Nicoloro, P. Furcinitti, C. Zhang, A. Chawla, J. Leszyk, and M. P. Czech.** 2003. Conventional kinesin KIF5B mediates insulin-stimulated GLUT4 movements on microtubules. EMBO J. **22:**2387–2399.
40. **Sztul, E., and V. Lupashin.** 2006. Role of tethering factors in secretory membrane traffic. Am. J. Physiol. Cell Physiol. **290:**C11–C26.
41. **Tengholm, A., M. N. Teruel, and T. Meyer.** 2003. Single cell imaging of PI3K activity and glucose transporter insertion into the plasma membrane by dual color evanescent wave microscopy. Sci. STKE **2003:**PL4.
42. **van Dam, E. M., R. Govers, and D. E. James.** 2005. Akt activation is required at a late stage of insulin-induced GLUT4 translocation to the plasma membrane. Mol. Endocrinol. **19:**1067–1077.
43. **Watson, R. T., M. Kanzaki, and J. E. Pessin.** 2004. Regulated membrane trafficking of the insulin-responsive glucose transporter 4 in adipocytes. Endocr. Rev. **25:**177–204.
44. **Watson, R. T., A. H. Khan, M. Furukawa, J. C. Hou, L. Li, M. Kanzaki, S. Okada, K. V. Kandror, and J. E. Pessin.** 2004. Entry of newly synthesized GLUT4 into the insulin-responsive storage compartment is GGA dependent. EMBO J. **23:**2059–2070.
45. **Yang, J., and G. D. Holman.** 1993. Comparison of GLUT4 and GLUT1 subcellular trafficking in basal and insulin-stimulated 3T3-L1 cells. J. Biol. Chem. **268:**4600–4603.
46. **Zeigerer, A., M. A. Lampson, O. Karylowski, D. D. Sabatini, M. Adesnik, M. Ren, and T. E. McGraw.** 2002. GLUT4 retention in adipocytes requires two intracellular insulin-regulated transport steps. Mol. Biol. Cell **13:**2421–2435.
47. **Zeigerer, A., M. K. McBrayer, and T. E. McGraw.** 2004. Insulin stimulation of GLUT4 exocytosis, but not its inhibition of endocytosis, is dependent on RabGAP AS160. Mol. Biol. Cell **15:**4406–4415.
48. **Zenisek, D., J. A. Steyer, M. E. Feldman, and W. Almers.** 2002. A membrane marker leaves synaptic vesicles in milliseconds after exocytosis in retinal bipolar cells. Neuron **35:**1085–1097.